Geochemistry, Geophysics, Geosystems

Supporting Information for

Generic along-strike segmentation of Afar normal faults, East Africa: Implications on fault growth and stress heterogeneity on seismogenic fault planes

Manighetti I.[(1)], Caulet C.[(1)], De Barros L.[(1)], Perrin C.[(1)], Cappa F.[(1)], and Gaudemer Y.[(2)]

(1) Université Nice Sophia-Antipolis, CNRS, IRD, Observatoire de la Côte d'Azur, Geoazur UMR 7329, 250 rue Albert Einstein, Sophia Antipolis, 06560 Valbonne, France

(2) Institut de Physique du Globe de Paris, 1 rue Jussieu, 75238 Paris cedex 05, France

Contents of this file

Introduction

This supporting information provides additional figures to the main article, dedicated to provide details on a few specific points discussed in the main text.

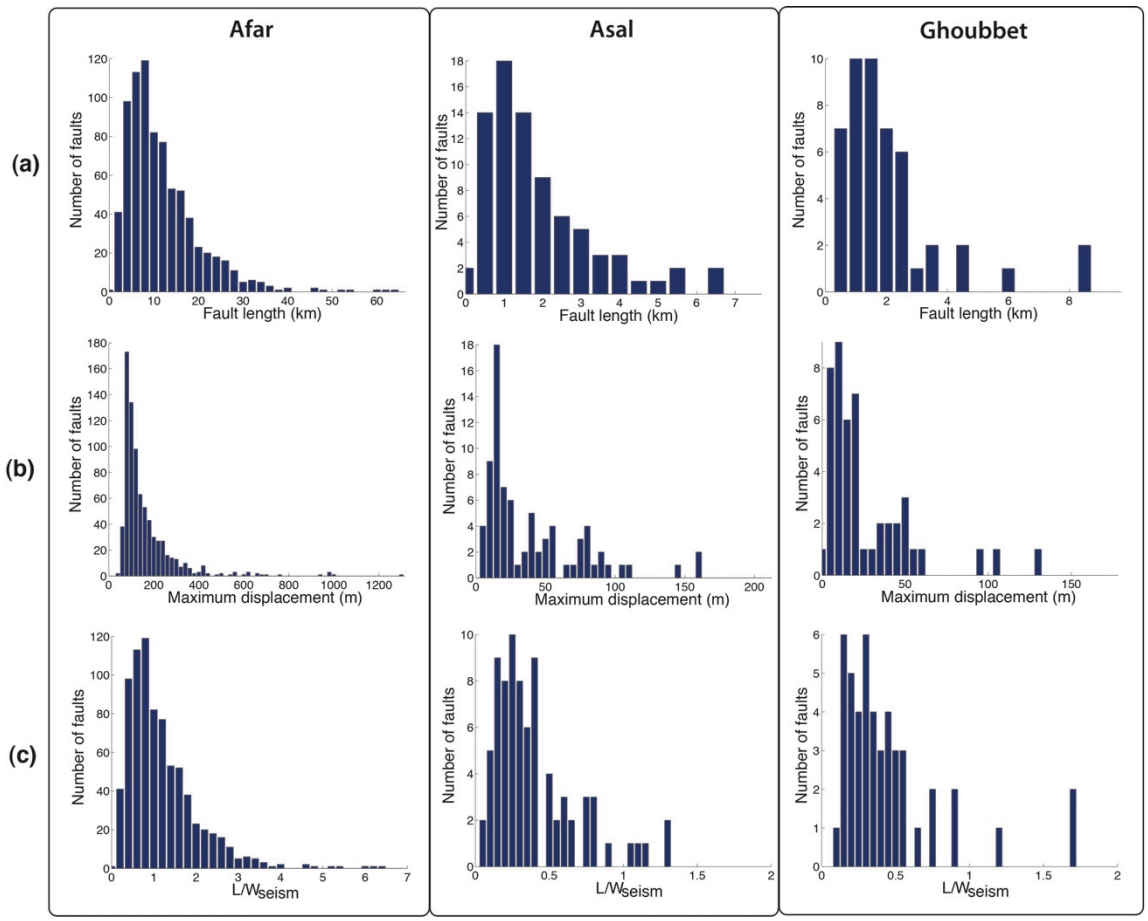

Figure S1. Distribution of lengths, maximum cumulative displacements, and length to seismogenic crust thickness ratios for fault populations from the Afar, Asal, and Ghoubbet areas. (a) Length distribution; (b) Maximum cumulative displacement distribution; (c) Distribution of fault lengths relative to seismogenic crust thickness (W_{seism}).

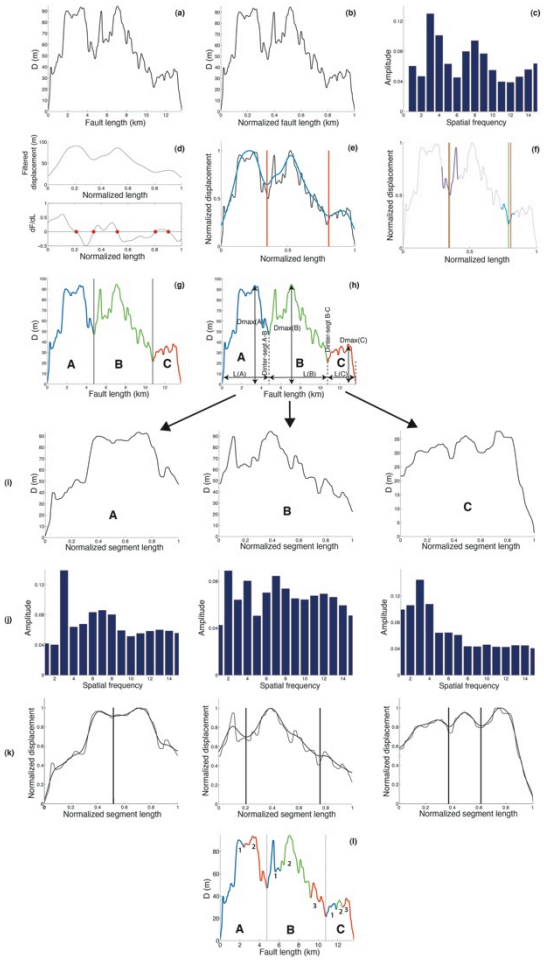

Figure S2. Processing chain of the filtering method (see section 3). (a) Raw cumulative fault displacement profile (fault # S498). (b) Normalized fault displacement profile. (c) Histogram showing the spectral amplitude of the S-transform at the various spatial frequencies. The largest amplitude is found at a spatial frequency of 3, which suggests that the fault displacement profile contains three major peaks and hence that the fault contains three major segments. (d) Filtering of the fault displacement profile with a cut-off frequency of 6, and then derivation of the filtered profile. The derivation allows locating along the fault the zones of local minimum displacement that coincide with the major inter-segments. (e) Position on the actual normalized fault profile of the major segment edges (red) defined in (d) and shown in the filtered profile in blue. The segment edge (inter-segment) farthest to the right does not coincide exactly with the actual minimum displacement zone. (f) Search of the actual minimum displacement zones closest to the major segment limits defined in (d-e). The search is made among 15% of the data points (colored zones on the profile) on either side of the limit (inter-segment) identified in the filtered profile. The actual minimum displacement zones are found and indicated in green. (g) Three major segments are identified with the filtering approach described above. They are reported on the actual fault profile and numbered A-B-C in direction of overall cumulative displacement decrease. (h) Once the major segments are identified, we can measure their individual length (L_i), their maximum cumulative displacement ($D_{max\text{-}i}$), and the cumulative displacement at the major inter-segments ($D_{inter\text{-}segt\ i\text{-}j}$). The entire chain of process is then repeated on individual major segment profiles to identify and measure the secondary segments within each of these major segments. (i) Normalized displacement profiles of each of the three identified A-B-C major segments. (j) S-transform histograms showing the spatial frequencies of the displacement oscillations in each of the 3 A-B-C major segment profiles. (k) Position on both the filtered (F_c= 6) and the actual major segment profiles of the secondary segment edges (vertical lines) defined through derivation of the filtered profiles. (l) Final result showing both the major (A-B-C) and the secondary (blue, green and red and small numbers) segments within the fault (actual profile)

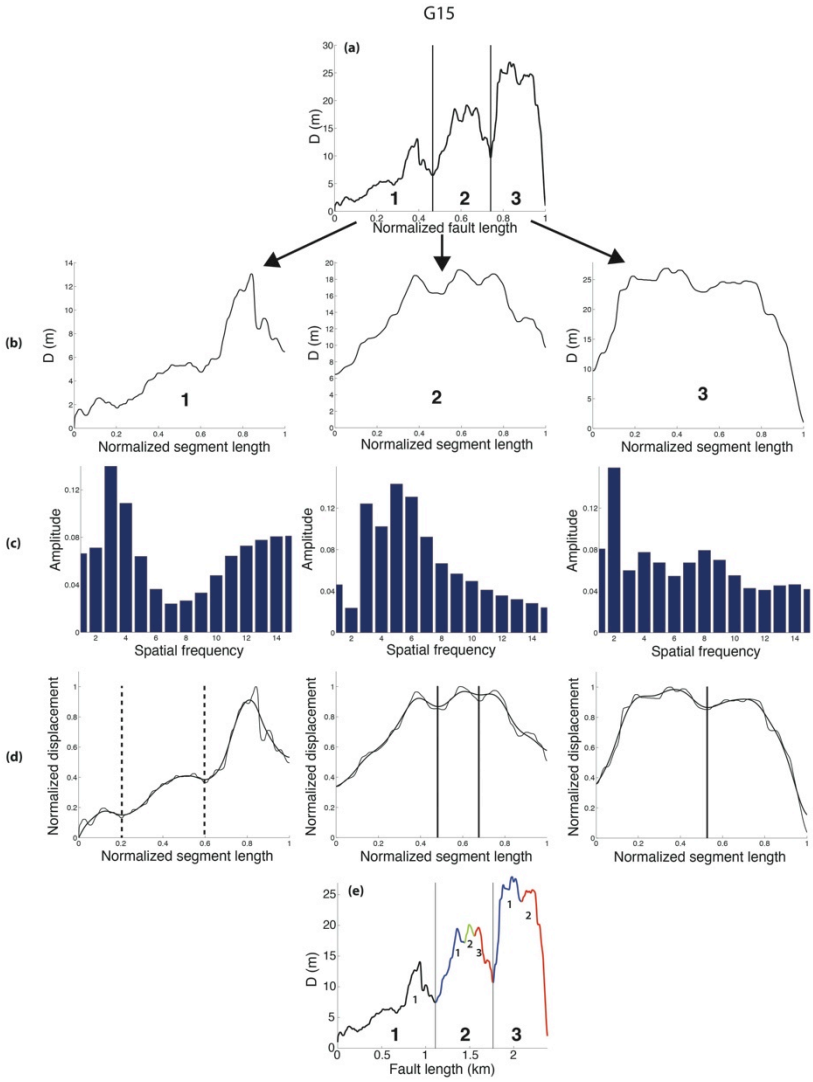

Figure S3. Processing for secondary segment identification in fault G15 shown in Fig. 4. (a) Normalized fault profile with the 3 major segments identified (1-2-3 separated with vertical lines); (b) Normalized displacement profiles of each of the three 1-2-3 major segments; (c) S-transform histograms showing the spatial frequencies of the displacement oscillations in each of the 3 major segment profiles. (d) Position on both the filtered (F_c= 6) and the actual major segment normalized profiles of the secondary segment edges (vertical lines) defined through derivation of the filtered major segment profiles. The dotted vertical lines in major segment 1 indicate secondary troughs and hence secondary inter-segments which can be seen in the profile, yet that were not detected with the filtering approach. (e) Final result showing both the major (1-2-3) and the secondary segments (blue, green, red and black, and small numbers) within the fault (actual profile). The G15 example shows different situations: for major segment 1, the S-transform approach well identifies the 3 secondary segments whereas the filtering approach fails to detect them; for major segment 2, the filtering approach well identifies the 3 secondary segments whereas the S-transform approach fails to detect them; for major segment 3, both the S-transform and the filtering approaches well identify the 2 secondary segments

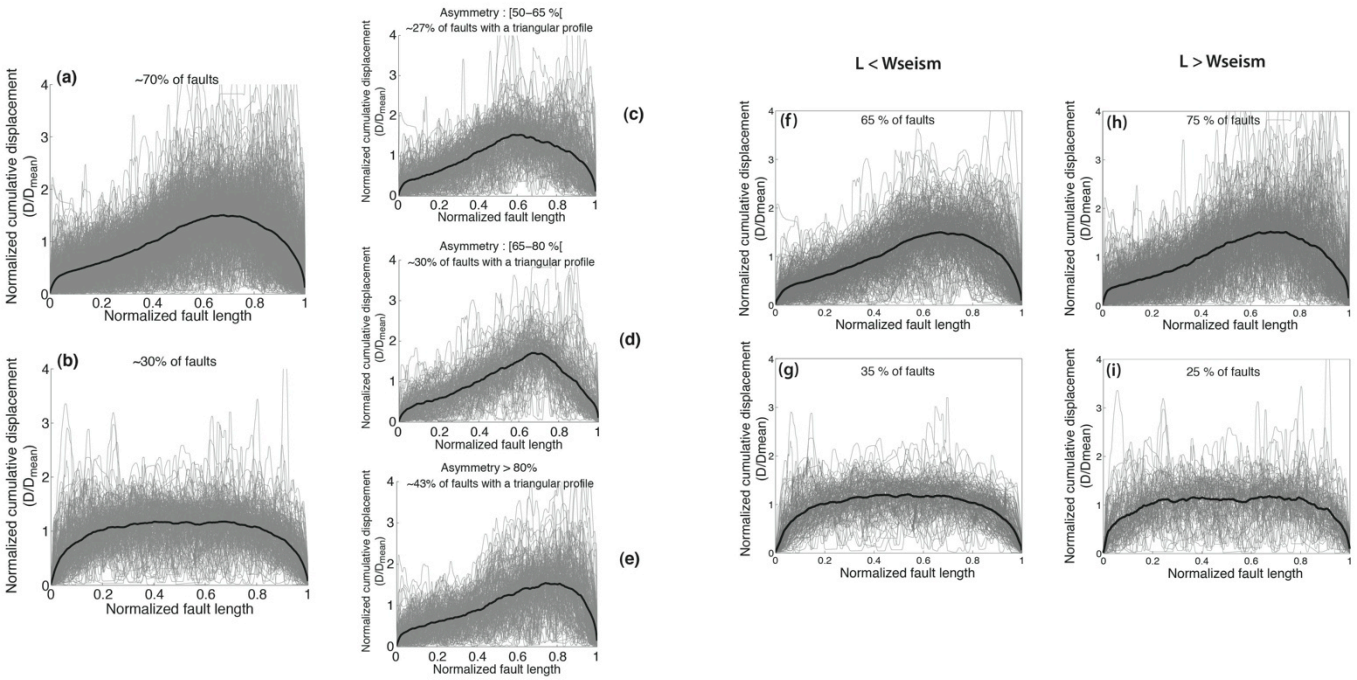

Figure S4. Envelope shape of cumulative displacement-length profiles for the entire fault population. Profiles, in grey, have been normalized to both fault length and mean cumulative displacement. Some profiles have been shifted to place the maximum displacement at the right. A best-fit average curve is shown as a thick black line. (a) ~70 % of the faults show a triangular and asymmetric cumulative displacement-length profile. (b) ~30 % of the faults show a fairly elliptical cumulative displacement-length profile. The root-mean-squared values for the best-fitting triangular and elliptical functions show that many of the fault profiles best-adjusted with an elliptical function are fitted almost as well with a triangular function. Therefore, faults having a triangular displacement profile may be even more numerous than the ~70 % suggested above. Among faults with a triangular profile, ~27 % have their displacement-length profile fairly symmetric (degree of asymmetry of best-fitting triangular function (below simply referred to as 'asymmetry') between 50 and 65 % of fault length; Fig. 4c), ~30 % have their displacement-length profile moderately asymmetric (asymmetry between 65 and 80 % of fault length; Fig. 4d), and ~43 % have their displacement-length profile strongly asymmetric (asymmetry > 80 % of fault length; Fig. 4e). The triangular shape of the cumulative displacement profiles is independent on whether the fault length is less or greater than the seismogenic crustal thickness (Fig. 4 f-g: L < Wseism; Fig. 4 h-i: L > Wseism), and hence independent also of the fault location and of the DEM resolution (Fig. 4 f-g-h-i).

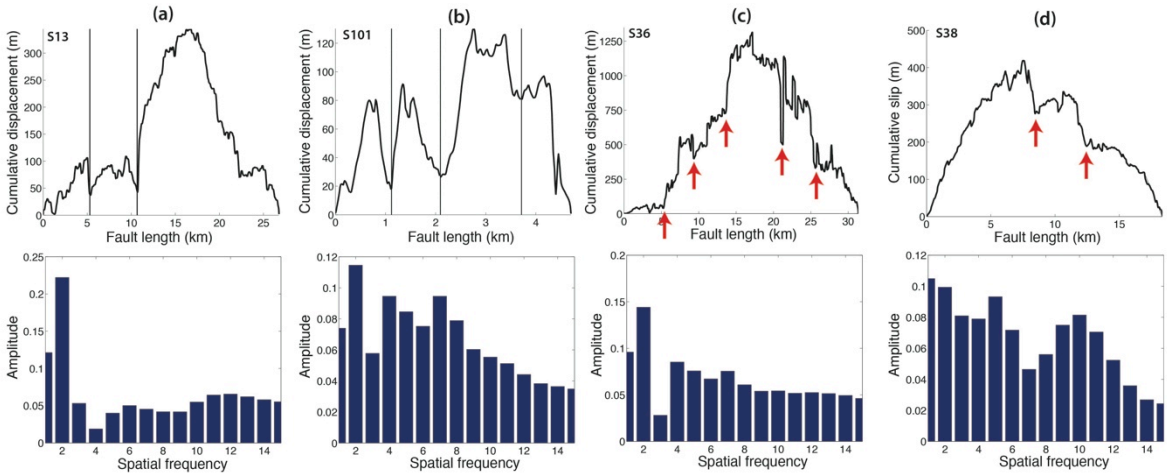

Figure S5. Examples of fault displacement profiles in which the lateral segmentation was not fully revealed by the signal processing methods. (a) and (b) example-profiles found to be divided into two major segments with the S-transform approach (see histograms in lower panels), whereas they clearly have a richer low frequency displacement content, well revealed with the filtering method (black vertical lines). (c) and (d) example-profiles classified as "un-segmented" with the filtering approach (and also with the S-transform approach for case d), whereas they actually show a fairly clear large-scale segmentation indicated with the red arrows.

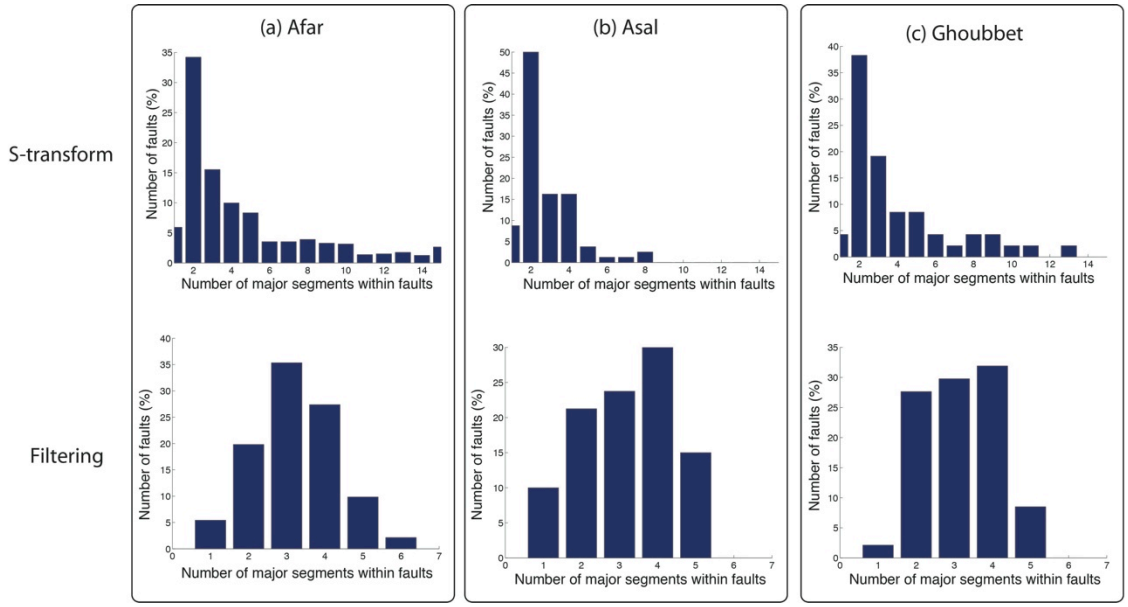

Figure S6. Number of major segments within faults when the latter are discriminated by their location.

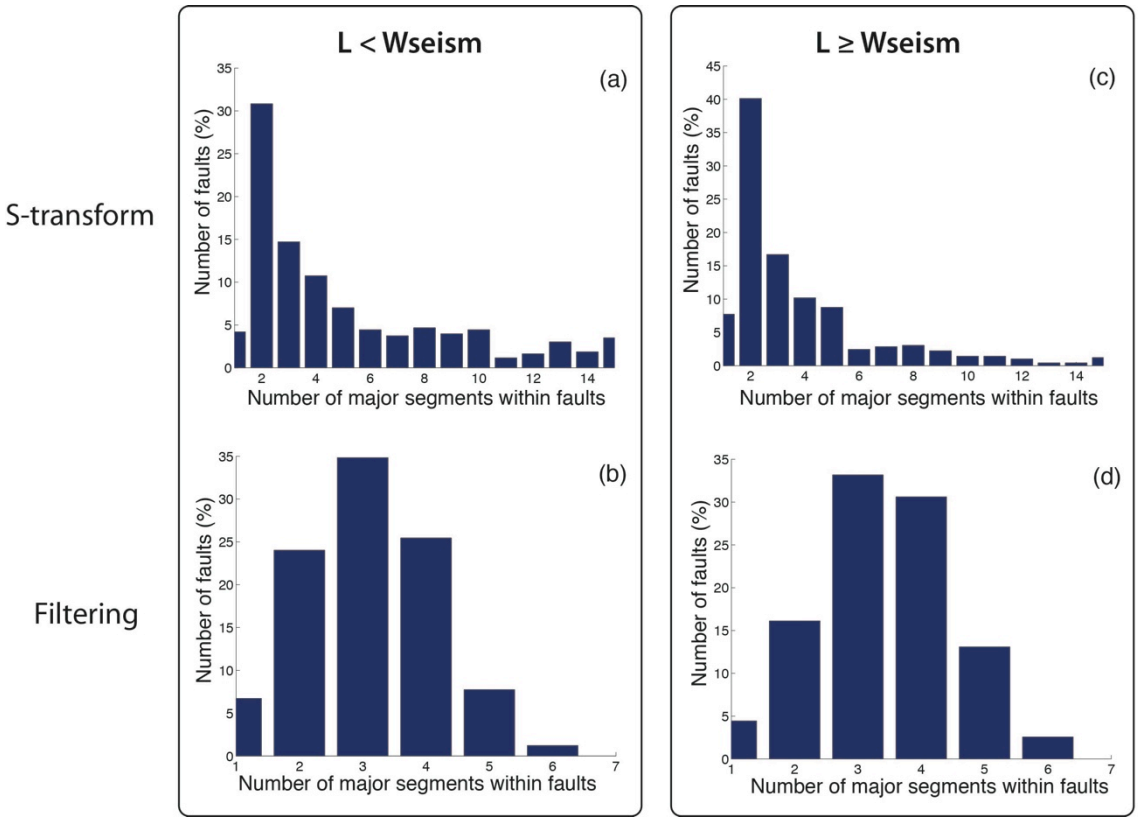

Figure S7. Number of major segments within faults when the latter are discriminated from having a length less or greater than the seismogenic crust thickness.

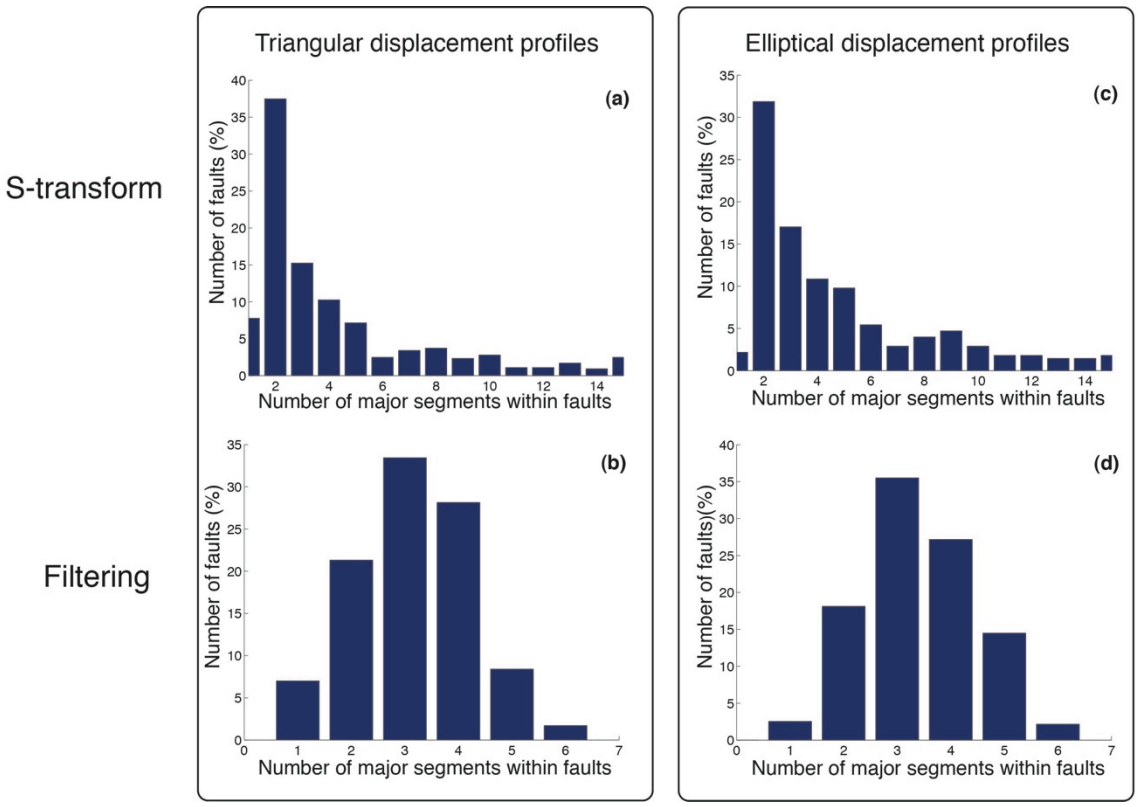

Figure S8. Number of major segments within faults when the latter are discriminated by the envelope shape of their cumulative displacement profile.

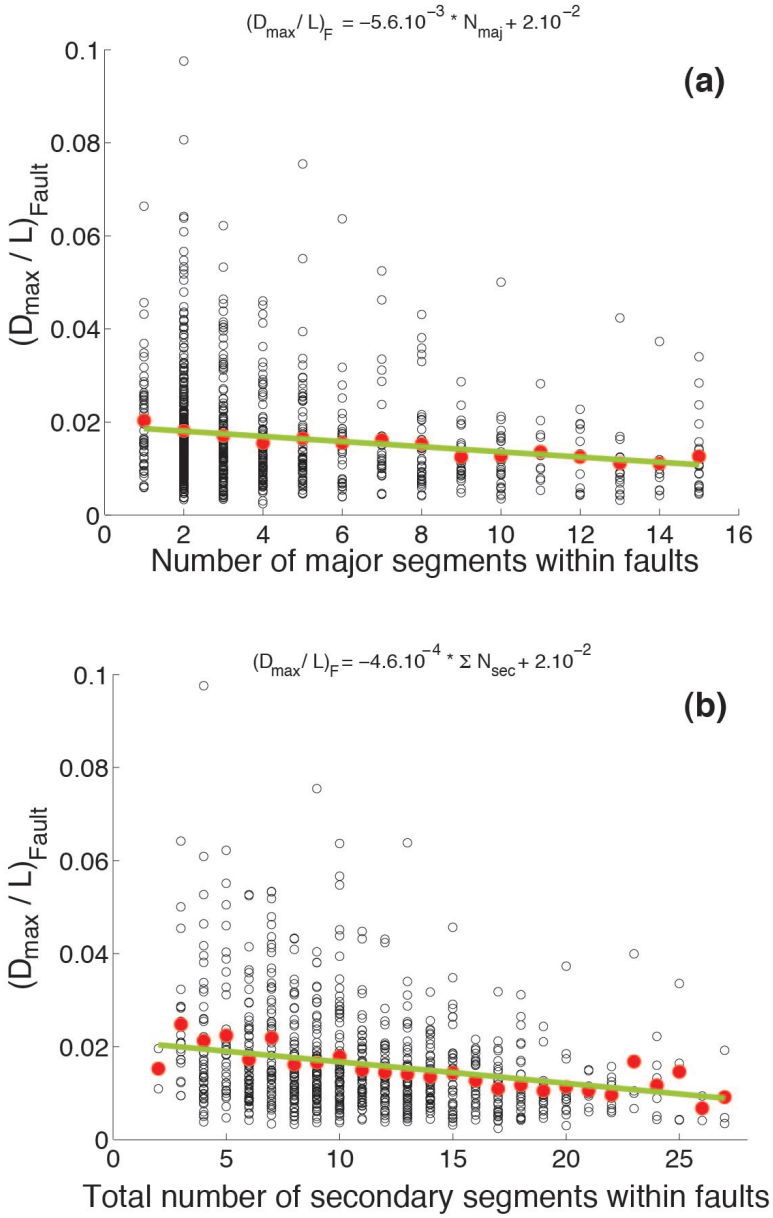

Figure S9. Same as Figure 6 but with major and secondary segment numbers derived from S-transform approach. (a) Number of major segments within faults (N_{maj}) as a function of maximum displacement to length ratio of the faults $(Dmax/L)_F$ ($R^2 = 0.93$). (b) Total number of secondary segments within faults ($SumN_{Sec}$) as a function of maximum displacement to length ratio of the faults $(Dmax/L)_F$ ($R^2 = 0.8$). In all cases, individual data are in black circles, their average values in red, and the linear regression scaling (green line) is the calculated fit to average values.

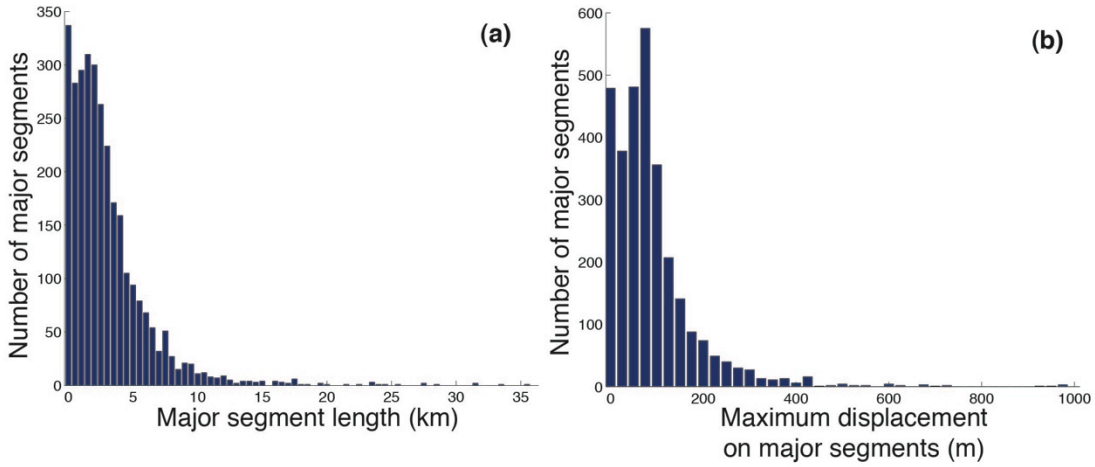

Figure S10. Distribution of major segment lengths and maximum cumulative displacements (lengths and maximum displacements measured as in Supp. Fig. 2h; un-segmented profiles ignored from the graphs).

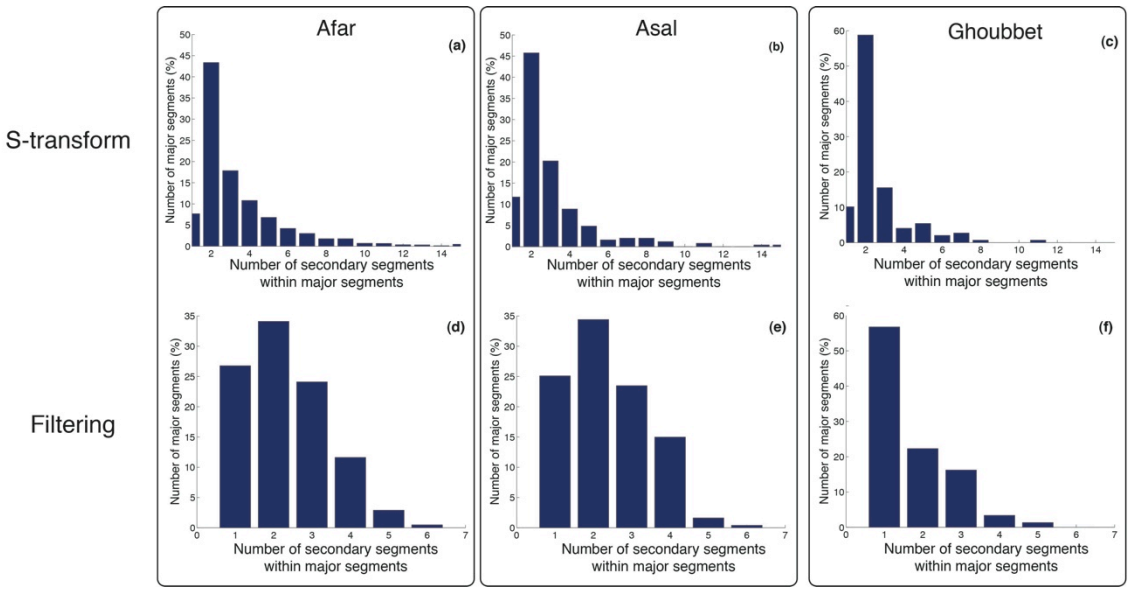

Figure S11. Number of secondary segments within major segments when faults are discriminated by their location.

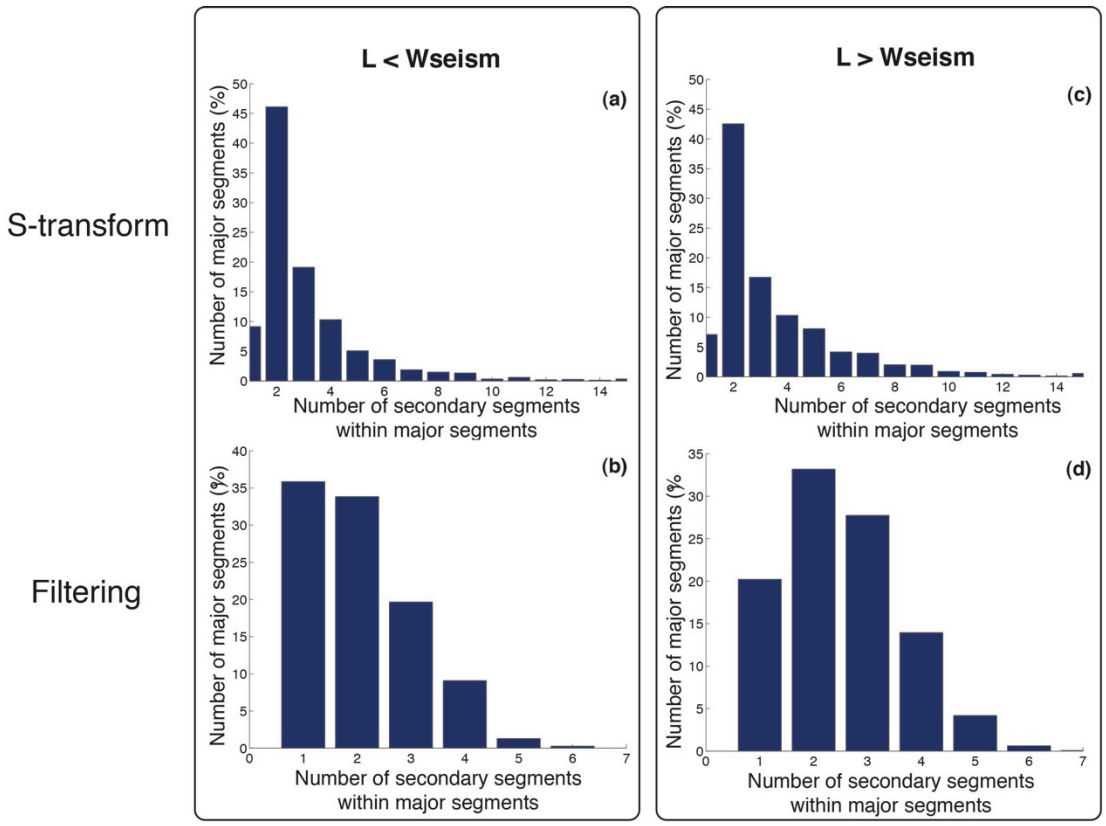

Figure S12. Number of secondary segments within major segments when faults are discriminated from having a length less or greater than the seismogenic crust thickness.

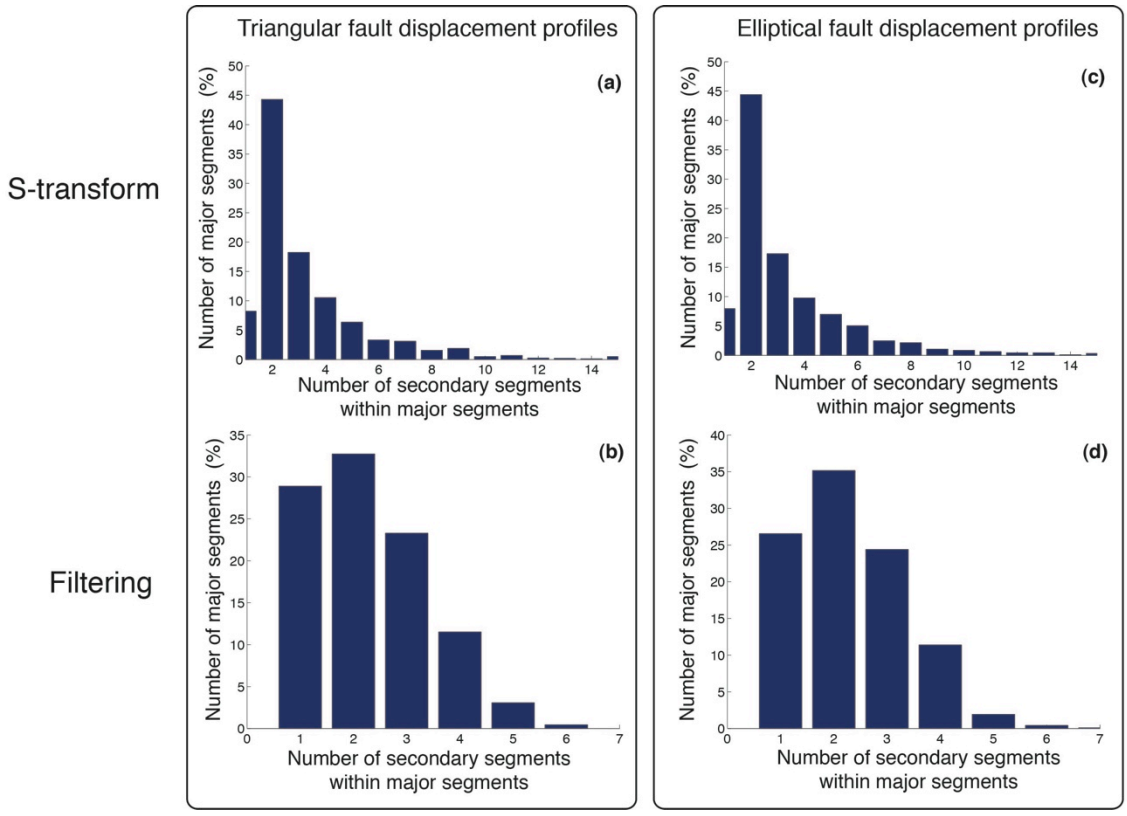

Figure S13. Number of secondary segments within major segments when faults are discriminated from the envelope shape of their cumulative displacement profile.

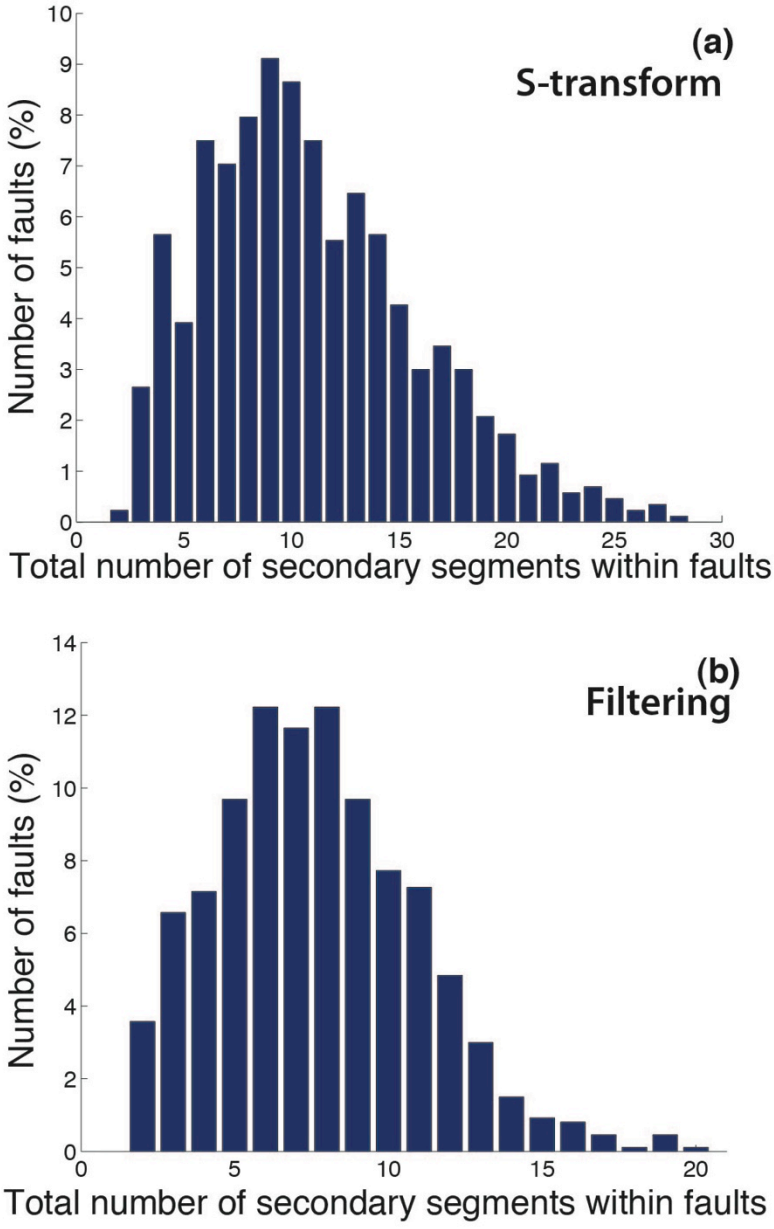

Figure S14. Total number of secondary segments within faults. (a) Derived from S-transform. (b) Derived from filtering method.

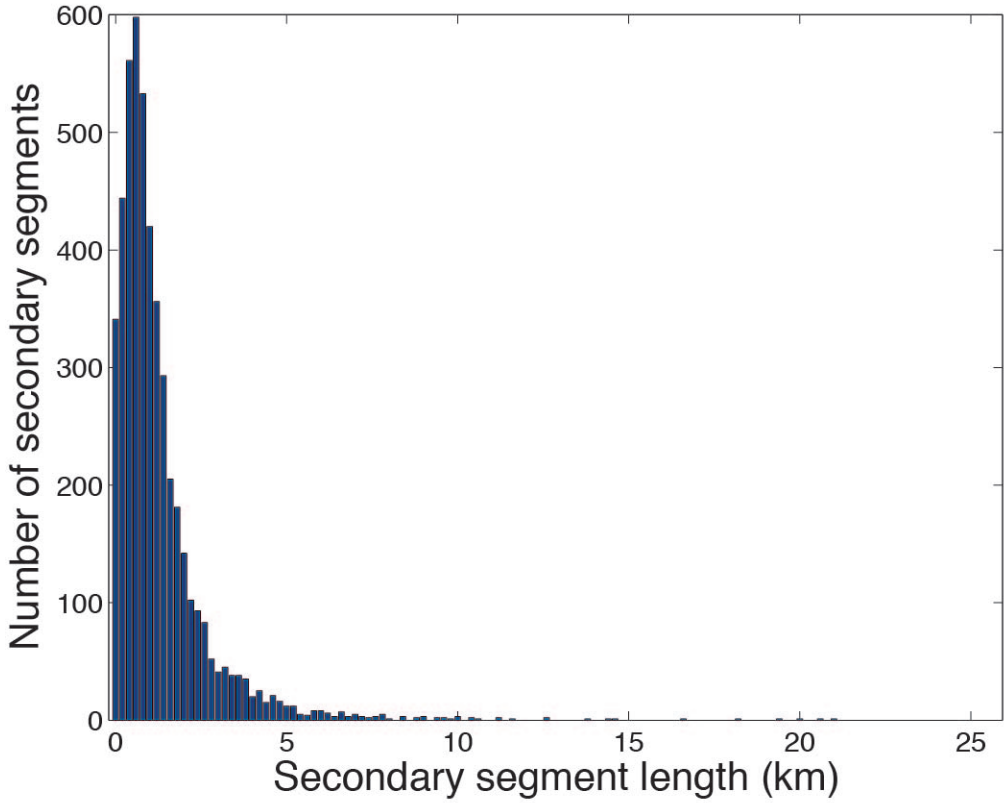

Figure S15. Distribution of the lengths of the secondary segments (un-segmented profiles omitted from the graph).